

Climatological Characteristics of Typical Daily Precipitation

ANGELINE G. PENDERGRASS AND CLARA DESER

National Center for Atmospheric Research,^a Boulder, Colorado

(Manuscript received 20 September 2016, in final form 12 April 2017)

ABSTRACT

Precipitation is often quantified by the amount that falls over a given period of time but not the rate at which most of it falls or the rate associated with the most frequent events. Here, three metrics are introduced to distill salient characteristics of typical daily precipitation accumulation based on the full distribution of rainfall: rain amount peak (the rain rate at which the most rain falls), rain frequency peak (the most frequent nonzero rain rate), and rain amount width (a measure of the variability of typical precipitation accumulation). These metrics are applied to two observational datasets to describe the climatology of typical daily precipitation accumulation: GPCP 1° daily (October 1996–October 2015) and TMPA 3B42 (January 1998–October 2015). Results show that the rain frequency peak is similar to total rainfall in terms of geographical pattern and seasonal cycle and varies inversely with rain amount width. In contrast, the rain amount peak varies distinctly, reaching maxima on the outer edges of the regions of high total precipitation, and with less seasonal variation. Despite that GPCP and TMPA 3B42 are both merged satellite–gauge precipitation products, they show substantial differences. In particular, the rain amount peak and rain amount width are uniformly greater in TMPA 3B42 compared to GPCP, and there are large discrepancies in their rain frequency distributions (peak and width). Issues relating to model evaluation are highlighted using CESM1 as an illustrative example and underscore the need for observational datasets incorporating measurements of light rain.

1. Introduction

How much rain falls on a typical rainy day? The most common metric used to quantify precipitation is its average over a period of time—a month, season, or longer. This metric suffices to differentiate the wettest locations from the driest ones; for example, the western Pacific warm pool has higher mean rainfall than the Sahara. Because rainfall varies within each year, season, and month, total precipitation does not describe the precipitation of a typical rainy day.

Precipitation frequency quantifies how often it rains (Englehart and Douglas 1985). The total frequency and total intensity of rain (which is the total precipitation divided by the frequency of precipitation) provide aggregate measures of how often it rains and how heavy this rain is. Some studies have examined total frequency

and intensity in observations (Chen et al. 1996; Sun et al. 2006; Dai et al. 2007; Biasutti and Yuter 2013). Intercomparison of observational datasets reveals large uncertainty in precipitation products (Gehne et al. 2016; Herold et al. 2016). Model evaluation in terms of total frequency and intensity shows that models rain too often and not hard enough (Stephens et al. 2010).

Extreme precipitation metrics quantify how heavy the heaviest rainfall events are. Some examples include the heaviest day of precipitation in a season or year and the precipitation rate at a particular (extreme) percentile of the distribution. Because extreme precipitation can cause floods, it is the focus of much literature (e.g., Ricko et al. 2016). However, extreme events are by definition infrequent and atypical.

Analyzing the distribution of rain in terms of rain rate enables a distinction to be made between light and heavy precipitation events. The distribution of rain was first characterized qualitatively (Petty 1995; Dai 2001) or with categorical bins (e.g., Dai 2006). While much of this earlier work focused on the rain frequency distribution, Watterson and Dix (2003) calculated the amount of rain falling in each bin, which we will refer to as the rain

^aThe National Center for Atmospheric Research is sponsored by the National Science Foundation.

Corresponding author: Angeline G. Pendergrass, apgrass@ucar.edu

amount distribution (other studies refer to it as the rain volume distribution; e.g., Behrangi et al. 2012). The rain amount distribution sums to the total precipitation. Sun et al. (2007) quantified the distribution of rain using bins spaced linearly in rain rate, which provide a basis for mathematical manipulation but have poor sampling properties (since daily precipitation accumulation spans orders of magnitude). Pendergrass and Hartmann (2014a) calculated the rain frequency and rain amount distributions with bins that are spaced logarithmically.

Changes in precipitation have also been the focus of a large body of work. Changes in precipitation have been detected in observations (e.g., Wentz et al. 2007; Min et al. 2011) and are projected by model simulations (e.g., Allen and Ingram 2002; Held and Soden 2006; Pall et al. 2007; Pendergrass and Hartmann 2014b).

Missing from the literature is a focus on typical precipitation events—events that occur most often and contribute the most precipitation and latent heating. Typical events do not have the sampling problem associated with extreme precipitation, and they are more often relevant. In contrast to total intensity and total precipitation, which aggregate over the entire distribution of rain, metrics for typical precipitation would put the focus on typical events. Here, we develop metrics to quantify characteristics of typical daily precipitation accumulation by distilling information from its distribution. We document the global spatial patterns of each metric, and compare them with the total rainfall. This is the first comprehensive study describing metrics applied to a global observational daily precipitation dataset, examining the seasonal cycle, and defining a width metric. Recent work by Kooperman et al. (2016) and Venugopal and Wallace (2016) have defined metrics similar to the rain amount peak (defined below) and examined them using TMPA 3B42 (introduced in section 2).

The rest of this study is organized as follows. Section 2 provides information on the datasets and methodology for computing the rainfall distributions and an illustrative example of how they are calculated. In section 3, we define the rain amount peak, rain frequency peak, and rain amount width metrics. In section 4, we apply the metrics to a global observational product; zonal-mean distributions are considered in section 4a, spatial patterns of rain amount peak and rain frequency peak in section 4b, and the rain amount width in section 4c. Comparison against one alternative observational product is included in section 5. Section 6 highlights issues relating to model evaluation and concerns regarding rain frequency. Discussion is provided in section 7 and concluding remarks in section 8.

2. Datasets and rain distribution methodology

a. Observational datasets and model simulation

Two global-scale gridded precipitation products with daily or higher temporal resolution based on satellite observations are available starting in the late 1990s: the Global Precipitation Climatology Project (GPCP) 1° daily (1DD) dataset (Huffman et al. 2001), and Tropical Rainfall Measuring Mission (TRMM) Multisatellite Precipitation Analysis (TMPA) 3B42 product, version 7 (hereafter TRMM 3B42; Huffman et al. 2007). Both datasets incorporate satellite measurements over land and ocean as well as gauge data over land to produce a gridded product. We include the entire temporal record from each product: October 1996–October 2015 for GPCP and January 1998–October 2015 for TRMM. GPCP has global coverage with 1° spatial resolution and daily temporal resolution. TRMM covers the region 50°N–50°S, with 0.25° spatial resolution and 3-hourly temporal resolution; we use the daily aggregated product and coarsen the data from its native 0.25° grid to a 1° grid for comparison with GPCP. Both datasets use IR satellite measurements of cloud-top brightness temperature as a proxy for rain rates when other data are unavailable. The measurement inputs to both datasets vary with latitude as a result of the satellite orbits, with infrared brightness temperature becoming increasingly important poleward of 40° [see Huffman and Bolvin (2013) with regard to GPCP]. TRMM also makes use of TRMM Precipitation Radar data. Both TRMM and GPCP include microwave measurements of precipitation, which require different treatments over land and ocean resulting from their differing surface emissivities (e.g., Kummerow and Giglio 1995).

We also use 10 years (1996–2005) of a twentieth-century historical simulation from Community Earth System Model, version 1 (CESM1; Hurrell et al. 2013), a comprehensive fully coupled climate model. In particular, we use data from the first member of the CESM1 30-member initial-condition ensemble (Kay et al. 2015). The resolution of this CESM1 simulation is approximately 1° in latitude and longitude, similar to GPCP's 1° resolution.

b. Calculating the distribution of rain

We compute the distributions of rain frequency and rain amount at each grid box using the full period of record available for each dataset. Following Pendergrass and Hartmann (2014a), we sort the daily precipitation data into bins that scale logarithmically with rain rate where each bin center is 7.67% bigger than the last, for a total of 140 bins. The lower edge of the first bin is set at $0.032 \text{ mm day}^{-1}$, while its upper edge is

0.035 mm day⁻¹. Subsequent bins follow this same pattern, where the upper edge of one bin is the lower edge of the next. The rain frequency distribution is the number of days in each bin normalized by the total number of days. The rain amount distribution is the sum of accumulated precipitation in each bin normalized by the total number of days. More details of the methodology and a mathematical treatment of how we calculate the distributions of rain frequency and rain amount can be found in [Pendergrass and Hartmann \(2014a\)](#).

To obtain spatial averages of the distributions, we first area-weight the distributions at each grid box and then average the area-weighted distributions. To calculate averages over land and ocean separately, we use a land mask based on topographic data from [Amante and Eakins \(2009\)](#); if a grid box contains both land and ocean, we consider it to be land. The values of the rain amount and rain frequency distributions depend on the spatial and temporal resolution of the input data and on the bin width. Our focus will be on drawing qualitative conclusions from the datasets, which are not sensitive to the resolution or the bin width.

To illustrate how the rain frequency and rain amount distributions are constructed, we consider the time series of daily precipitation accumulation for the months of April and May of 2015 in Boulder, Colorado, obtained from Global Historical Climatology Network's daily station data archive ([Menne et al. 2012a,b](#)). Throughout the text, we refer to daily precipitation accumulation as rain rate following [Pendergrass and Hartmann \(2014a\)](#) or intensity following [Stone et al. \(2000\)](#). The time series of rain rate in Boulder is shown in [Fig. 1a](#). Days with no precipitation are indicated with light blue circles on the abscissa. Days with nonzero precipitation are marked with vertical bars; bar length indicates rain rate. Boxes along the top of [Fig. 1a](#) are color coded according to discrete rain-rate bins to visualize rain frequency ([Fig. 1b](#)), and bars are color coded to visualize rain amount ([Fig. 1c](#)). Note that the data for 5 May are missing. Over this two-month period, the total precipitation was 5.0 mm day⁻¹, equivalent to a total of 300 mm or approximately 12 in. (1 in. ≈ 25.4 mm), which is a wet spring for Boulder.

To quantify how often rain occurs at different rain rates, we construct the rain frequency distribution ([Fig. 1b](#)). Each bar of the rain frequency distribution is the number of days falling within each logarithmically spaced rain rate bin, divided by the total number of nonmissing days (60) in the time series. Days with less than 0.1 mm of precipitation are recorded as trace and considered dry for this example. The sum of the rain frequency distribution is 100%. No measureable

precipitation occurs on 45% of days. Precipitation between 0.1 and 1 mm day⁻¹ occurs on 13% of days, 27% of days have between 1 and 10 mm day⁻¹, and 15% of days have between 10 and 100 mm day⁻¹.

To quantify how much rain falls at different rain rates, we construct the rain amount distribution ([Fig. 1c](#)). Each bar of the rain amount distribution is the sum of all the rain falling within each rain-rate bin, normalized by the number of days in the time series, and can be visualized as proportional to the sum of all the bars of the corresponding color in [Fig. 1a](#). While the smallest nonzero bin contains over 10% of days, this bin contributes just 1.3% of the total precipitation because the rain rates are small. The moderate bin, with rain rates between 1 and 10 mm day⁻¹, contributes 24% of the total precipitation. While the heaviest bin has only 15% of days (10–100 mm day⁻¹), it includes 75% of the total precipitation. This example illustrates that days with heavy precipitation contribute disproportionately to the total precipitation, and the rain amount distribution emphasizes these heavy precipitation days.

3. Quantifying typical daily precipitation accumulation

The rain amount and rain frequency distributions describe how heavy rain is when it falls and how often it falls at different rain rates. The global, annual-mean rain amount and rain frequency distributions for GPCP are shown in [Fig. 2](#). The rain amount distribution is negatively skewed, with a longer tail at lighter rain rates compared to heavier rates ([Fig. 2a](#)). The rain frequency distribution ([Fig. 2b](#)) falls off less rapidly toward lighter rain rates than does the rain amount distribution, although it is also negatively skewed. The frequency of dry days (<0.1 mm day⁻¹) is 54%. We distill the characteristics of typical precipitation with three metrics that can be calculated from the distributions. Because these metrics focus on the peaks of the rain amount and rain frequency distributions, they convey information about the most common characteristics of rain; it is in this sense that we use “typical” to describe them.

The first metric is the rain amount peak. The rain amount peak is defined as the rain rate at which the maximum value of the rain amount distribution occurs. It is the rain rate at which the most rain falls. Returning to our example of the distribution of rain in Boulder, the rain amount peak would be on the order of 50 mm day⁻¹ (the maximum rain amount occurs in the bin with rain rates between 10 and 100 mm day⁻¹, and the coarse bins used for this illustrative example provide accuracy to only an order of magnitude). For the global annual mean GPCP rain amount distribution, this value is

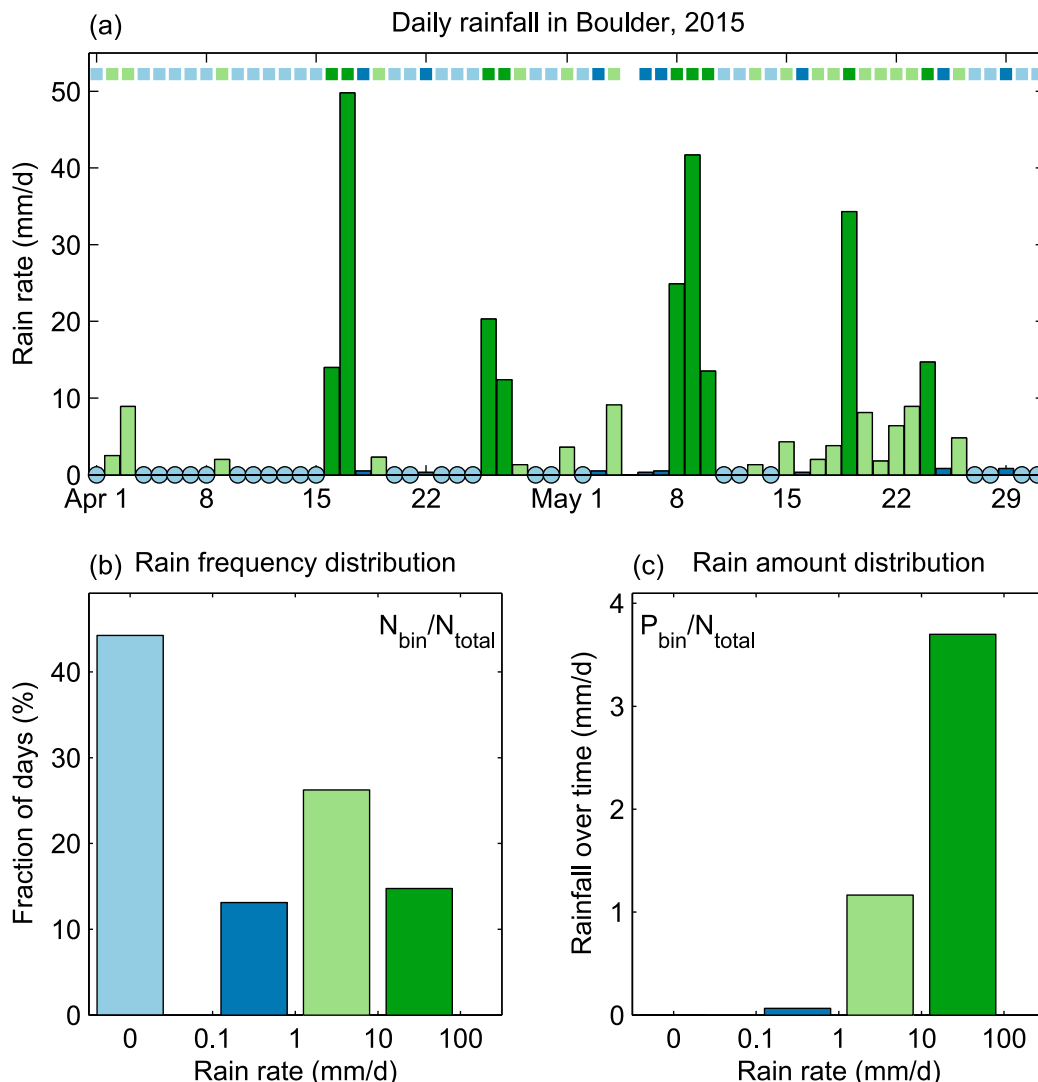


FIG. 1. Illustrative example of the calculation of the distributions of rain frequency and rain amount. (a) Time series of daily rainfall during 1 Apr–31 May 2015 at a station located in Boulder, Colorado. Daily precipitation accumulation (mm day^{-1}) indicated by bars, color coded by rain rate (dark green for values $>10 \text{ mm day}^{-1}$, light green for values between 1 and 10 mm day^{-1} , and dark blue for values $<1 \text{ mm day}^{-1}$). Light blue circles on the x axis indicate days when no measurable precipitation fell. The day with missing data is left blank. Colored boxes across the top also indicate the rain rate values using the same color scheme as the vertical bars. (b) The rain frequency and (c) rain amount histograms are calculated from the example time series.

18 mm day^{-1} (marked by a red star in Fig. 2a), which means that among all rain rates, the most rain falls at 18 mm day^{-1} .

The second metric is the rain frequency peak. Similarly to rain amount peak, rain frequency peak is defined as the rain rate where the maximum nonzero rain frequency occurs. It is the most frequent nonzero rain rate. In the global annual mean, the rain frequency peak is 5.5 mm day^{-1} (red star in Fig. 2b). Returning again to our Boulder example, the rain frequency peak is on the order of 5 mm day^{-1} (the bin between 1 and

10 mm day^{-1}). The global annual mean GPCP rain frequency distribution (Fig. 2b) has its peak at 5.5 mm day^{-1} , which is lower than the rain amount peak. The rain frequency distribution is centered at a lower rain rate than the rain amount distribution, reflecting the importance of heavy rain rates for total precipitation as we saw in the Boulder example (Fig. 1).

In addition to its peak, we can quantify the width of the rain amount distribution. The rain amount width is defined as the range of rain rates spanned by the portion of the rain amount distribution where the most rain falls.

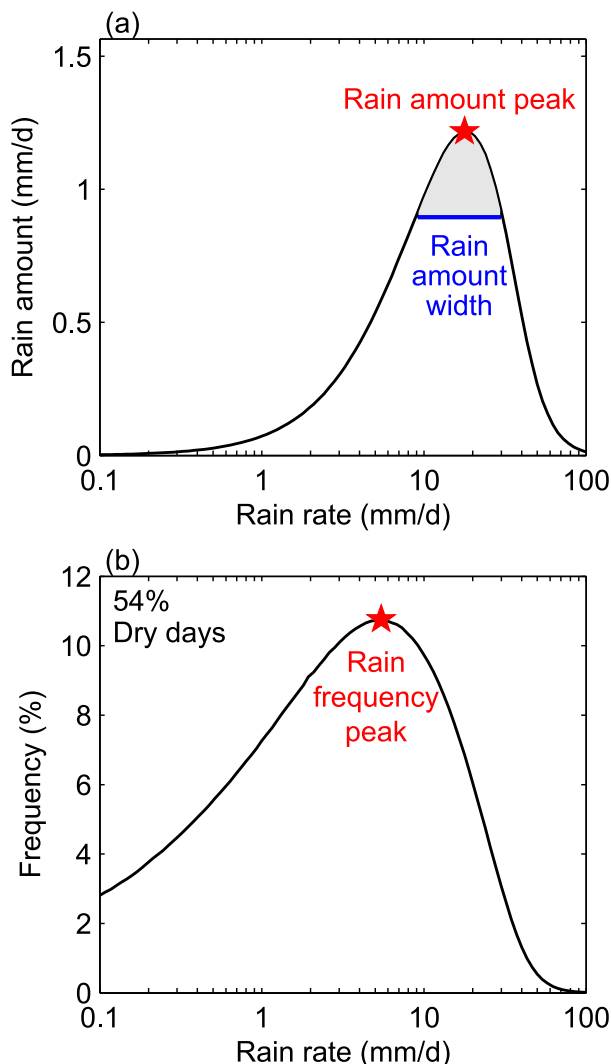


FIG. 2. The climatological distribution of global, annual mean (a) rain amount and (b) rain frequency from GPCP 1DD from October 1996 to October 2015. The red star denotes the rain amount peak in (a) and the rain frequency peak in (b). In (a), the horizontal blue line indicates the width of the rain amount distribution: see text for details. In (b), the dry-day frequency is given in the top left of the panel. This figure is updated from Pendergrass and Hartmann (2014a).

Specifically, the rain amount width is the ratio of the two rain rates where a line of constant rain amount intersects the rain amount distribution: it is expressed nondimensionally as the ratio of the greater to the lesser of these rain rates. We have chosen a width such that 10% of the total precipitation occurs in this portion of the rain amount distribution, as illustrated in Fig. 2a for the global annual mean. In the event that the rain amount distribution crosses the line of constant rain amount more than twice, the first rain rate it intersects on each side of the rain amount peak is chosen. The choice of

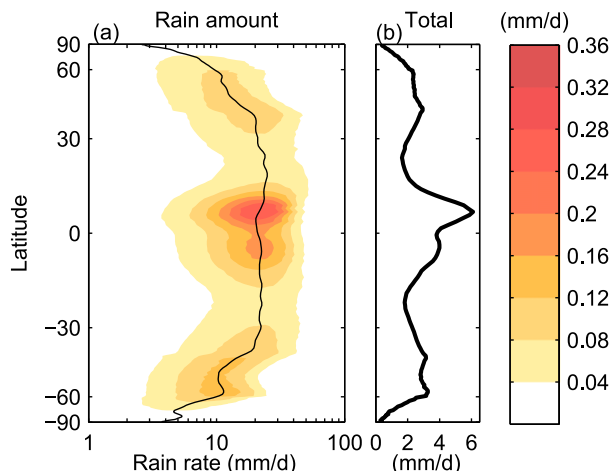


FIG. 3. (a) Climatological zonal, annual-mean rain amount (mm day^{-1}) distribution from GPCP 1DD based on data from October 1996 to October 2015. The black curve shows the rain amount peak at each latitude, smoothed with three successive applications of a 1–2–1 filter. (b) As in (a), but for total precipitation (mm day^{-1}) from the same dataset.

10% as a target fraction is arbitrary; we also tried 50%, which resulted in a change in magnitude but did not affect the geographical patterns or seasonal dependence. The rain amount width describes the range of rain rates where the most rain falls. The width of the global mean rain amount distribution is 2.2, indicating that 10% of the total precipitation falls between 9 and 30 mm day^{-1} .

We expect that the rain amount peak, rain frequency peak, and rain amount width will depend quantitatively but not qualitatively on the spatial and temporal resolution of the precipitation data from which they are computed. However, they do not depend systematically on the bin width, although the bin width does determine how accurate the metrics are (smaller bin widths provide finer granularity of the metrics, although they also require more sampling). We provide quantitative values of all three metrics, cognizant that they are specific to the spatial and temporal resolution of the particular datasets we examine.

4. The climatological distribution of rain in GPCP

a. The zonal-mean distribution of rain

We decompose the global mean rain amount distribution from GPCP into contributions from different latitudes in Fig. 3a. Note that the latitude axis is cosine weighted, proportional to the areal contribution of each latitude band. The peak of the rain amount distribution at each latitude is delineated by the thin black curve. Integration of the rain amount distribution at each

latitude over all rain rates yields the zonal-mean profile of total precipitation shown in Fig. 3b. Alternatively, integration over all latitudes at each rain rate produces the global mean rain amount distribution shown in Fig. 2a.

The rain amount distribution reaches a maximum at 22 mm day^{-1} and 6.5°N , the same latitude where the highest total precipitation occurs. A secondary maximum occurs at 22 mm day^{-1} and 3.5°S . The subtropical dry zones are characterized by both low total precipitation and low rain amount. However, the rain amount peaks in the subtropics are remarkably similar to those in the wetter tropics ($24\text{--}26 \text{ mm day}^{-1}$). Secondary maxima of the rain amount distribution occur in the midlatitudes ($30^\circ\text{--}60^\circ$ in both hemispheres) associated with the storm tracks. At the equatorward side of the storm tracks, the rain amount peak remains similar to tropical and subtropical values. Equatorward of 40° latitude, the rain amount peak varies between 19 and 26 mm day^{-1} , while the total precipitation spans a wider range, from 1.7 to 6.1 mm day^{-1} . Poleward of 40° latitude, the rain amount peak decreases with increasing latitude to about 10 mm day^{-1} at 60° latitude in both hemispheres; however, the GPCP data are less reliable here.

In summary, despite large variations in total rainfall and rain amount with latitude, the rain amount peak remains largely invariant equatorward of 40° and decreases by only a factor of 2 between 40° and 60° latitude. This implies that the intensity of typical daily precipitation varies little equatorward of 40° latitude, although below we will see that the rain amount peak has a rich longitudinal structure. Thus, zonal-mean statistics may be misleading in that they do not reveal the whole picture. The near-constant rain amount peak could not have been anticipated from total precipitation.

We might expect to find different rain amount distributions over ocean and land, because of a variety of physical factors including surface temperature, moisture, surface roughness, and related differences in atmospheric circulation or because of differences in the input data streams discussed in section 2. The zonal-mean rain amount distribution separated into ocean and land is shown in Fig. 4 (a gray line at 10 mm day^{-1} is included as a visual point of reference). Since ocean makes up two-thirds of Earth's surface, the distribution of rain amount over ocean (Fig. 4a) generally resembles the global mean at most latitudes (Fig. 3a). Over land (Fig. 4b), however, there are some notable differences from the global and ocean-only distributions. For example, the tropics show a single broad maximum centered near the equator, in contrast to the two separate maxima on either side of the equator over ocean. The

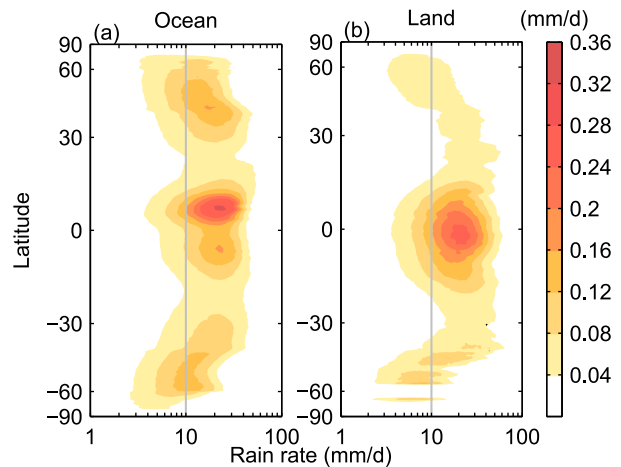


FIG. 4. As in Fig. 3a, but for (a) ocean and (b) land separately.

highest tropical rain amount is only slightly lower over land than ocean and occurs at a similar rain amount peak of $20\text{--}30 \text{ mm day}^{-1}$. Outside of the tropics, rain amounts are generally lower, and the distribution spans a narrower range of rain rates compared to ocean. Although values in the SH must be interpreted with caution as a result of the small amount of land at these latitudes, the rain amount distribution shows a secondary maximum in the SH midlatitudes. Overall, the bulk of the rain amount distribution equatorward of 40° latitude spans a similar range of rain rates ($20\text{--}30 \text{ mm day}^{-1}$) over ocean and land.

Precipitation varies over the annual cycle, and we can capture some of this variation by stratifying the zonal-mean rain amount distributions by 3-month seasons (Fig. 5). Over ocean, the tropical rainfall belts migrate with the seasonal cycle, with maximum rain amount values occurring in the ITCZ located around 5°N in winter (DJF) and spring (MAM) and around 9°N in summer (JJA) and fall (SON; Figs. 5a–d). The ITCZ also has somewhat higher rain amount in boreal summer and fall than in winter and spring. Like the NH, the latitude of the SH tropical rain amount maximum also varies by only a few degrees throughout the year and is stronger in austral summer and fall than winter and spring. The subtropical dry latitudes over ocean also migrate with the seasons. These dry zones skip from the NH in DJF and MAM to the SH in JJA (and to a lesser extent SON). Local maxima in midlatitudes of each hemisphere are associated with the storm tracks. As is the case in the annual mean, most precipitation in the storm tracks falls at rain rates characteristic of the tropics. While the latitude of the storm tracks varies only slightly with the seasons, their strength as measured by the rain amount does change, particularly in the NH,

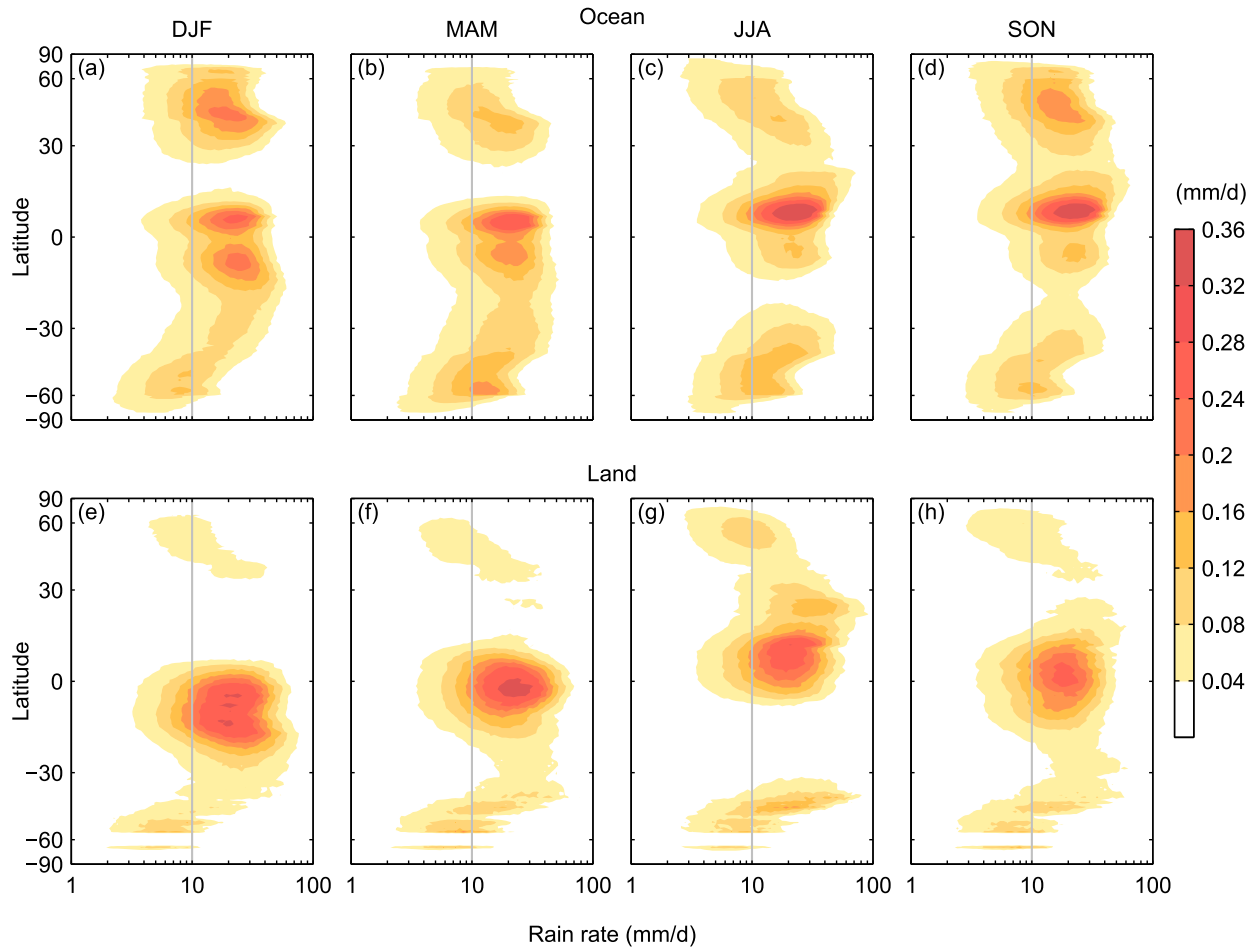


FIG. 5. As in Fig. 4, but stratified by season.

which shows largest values in fall and winter compared to spring and summer; the highest extratropical values in the SH occur in autumn.

The seasonal variation in zonal-mean rain amount over land (Figs. 5e–h) exhibits some general differences with that over ocean: there is one sole tropical maximum, its latitude migrates between 4.5°S in DJF and 11.5°N in JJA, and its strength is greatest in boreal spring. Other features are similar between ocean and land: the subtropical dry zone is present in austral summer, boreal winter, and boreal spring, and it encompasses a wider latitude band over land than over ocean; and midlatitude rain amount reaches a maximum in summer. Across all of these features, there is little variation in rain amount peak with the seasons, which is around 10 mm day^{-1} at $40^{\circ}\text{--}60^{\circ}\text{N}$ and $40^{\circ}\text{--}60^{\circ}\text{S}$ and $20\text{--}30\text{ mm day}^{-1}$ in the tropics and subtropics.

In summary, the zonal-mean rain amount distributions over both land and ocean show that the rate at which the most rain falls varies surprisingly little

through the seasonal cycle, over both land and ocean, between about 10 and 25 mm day^{-1} . In the next section, we will apply the rain amount peak, rain frequency peak, and rain amount width metrics to further explore the seasonal cycle and spatial pattern of typical daily precipitation at individual grid points.

b. Seasonal cycle and spatial pattern of rain amount peak and rain frequency peak

We can use the rain amount and rain frequency peak metrics to further distill the characteristics of the annual cycle of the zonal-mean rainfall distribution. Recall that the rain amount peak is the rain rate where the maximum value of the rain amount distribution occurs, and the rain frequency peak is the nonzero rain rate where the maximum of the rain frequency distribution occurs (see Fig. 2).

Figure 6 shows zonal-mean rain amount peak, rain frequency peak, total rainfall, and rain amount width as a function of latitude and month for ocean and land

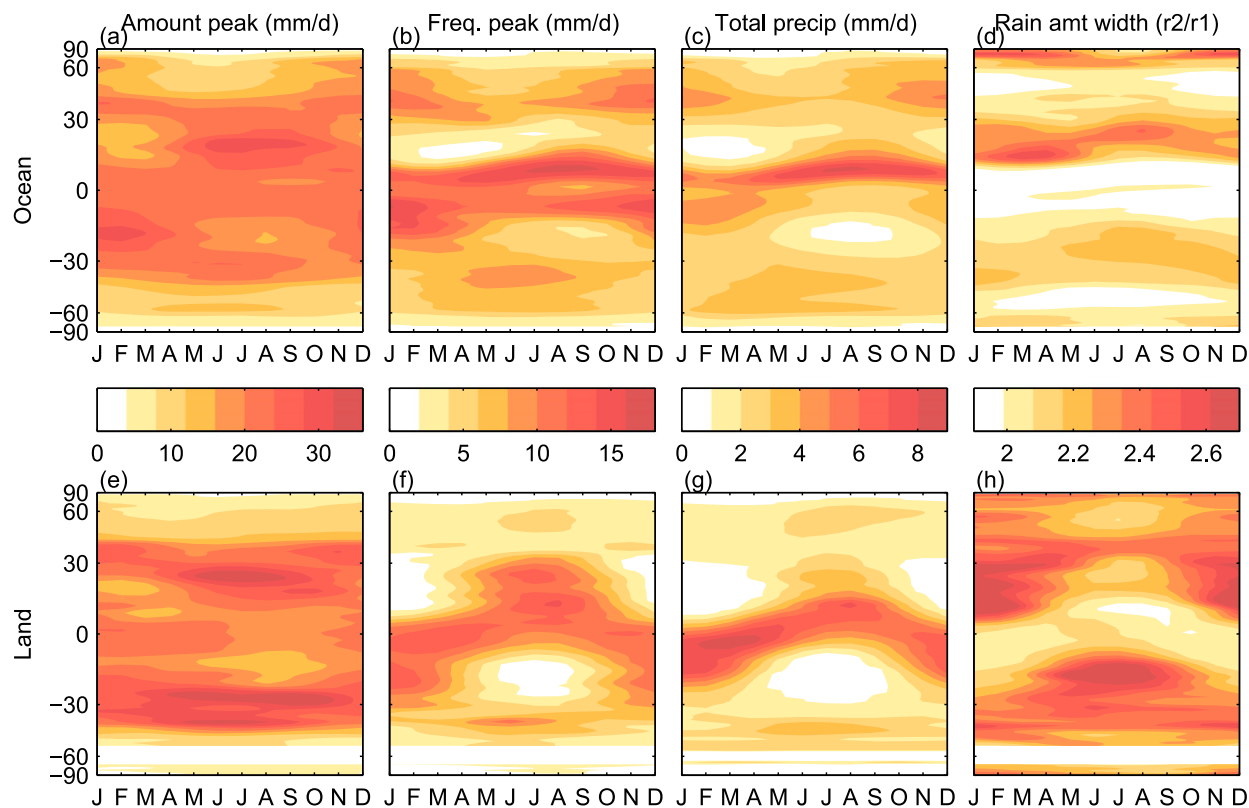


FIG. 6. Climatological zonal-mean distributions of (a),(e) rain amount peak, (b),(f) rain frequency peak, (c),(g) total precipitation, and (d),(h) rain amount width over (top) ocean and (bottom) land based on GPCP 1DD dataset for October 1996–October 2015. Rain amount peak, rain frequency peak, and rain amount width have been smoothed using a 3-point binomial filter, with three applications in latitude and two in month. Total precipitation is smoothed with the same filter applied once in latitude and once in month.

separately. Here we discuss the rain amount peak, rain frequency peak, and total rainfall; rain amount width is discussed in section 4c. The seasonal and latitudinal variations of the rain frequency peak are very similar to those of total precipitation, especially over land, and differ substantially from those of the rain amount peak. Rain amount peak has a weak seasonal cycle compared to rain frequency peak and total precipitation. This implies that the intensity of precipitation that contributes the most rain varies little over the course of the year compared to total precipitation and compared to the intensity of the most frequent precipitation.

Over ocean, there is a small annual cycle of rain amount peak (Fig. 6a) in the tropics ($<5 \text{ mm day}^{-1}$, with mean values of $20\text{--}25 \text{ mm day}^{-1}$). In contrast, the variations in the latitude and intensity of the ITCZ in the NH dominate the annual cycle for the rain frequency peak (Fig. 6b) and total precipitation (Fig. 6c), which both have annual cycles similar in magnitude to their annual mean values ($10\text{--}15 \text{ mm day}^{-1}$ for rain frequency peak and $3\text{--}6 \text{ mm day}^{-1}$ for total precipitation). In the subtropics, the rain amount peak reaches a maximum in

summer and a minimum in winter in each hemisphere, with an annual cycle of up to 15 mm day^{-1} compared to an annual mean value of $20\text{--}25 \text{ mm day}^{-1}$. For rain frequency peak and total precipitation, there are minima in spring, which are deeper in the NH compared to the SH. Their annual cycles remain similar in magnitude to annual mean values (around 10 mm day^{-1} for rain frequency peak and 3 mm day^{-1} for total precipitation). In mid-to-high latitudes, the annual cycle of rain amount peak, rain frequency peak, and total precipitation are all smaller than annual mean values by at least 50%. In the NH, there is a rain amount peak minimum in spring and summer and a maximum in fall and winter; the annual cycle is approximately 7 mm day^{-1} . Rain frequency peak and total precipitation also reach maxima during the winter months in each hemisphere, consistent with the seasonality of the storm tracks. In the SH mid- and high latitudes, the annual cycle is small for rain amount peak (less than 5 mm day^{-1}), rain frequency peak, and total precipitation.

Over land, a small annual cycle of rain amount peak (about 5 mm day^{-1} ; Fig. 6e) is present in the tropics, with

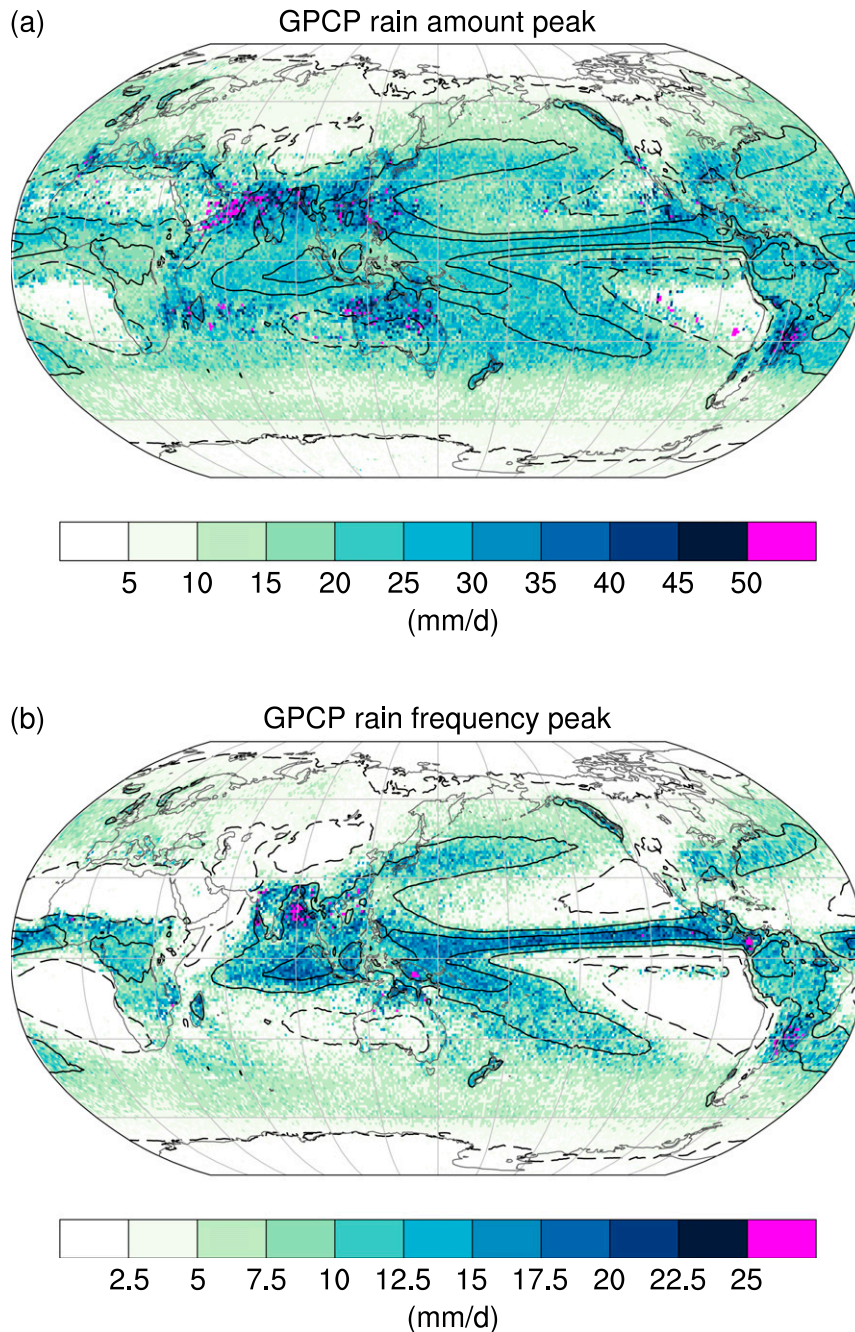


FIG. 7. Maps of climatological annual mean (a) rain amount peak and (b) rain frequency peak from GPCP 1DD (color shading; mm day^{-1}), with total precipitation indicated in black contours (1 mm day^{-1} is dashed, and 4 and 7 mm day^{-1} are solid).

lower values from July through October and little migration in latitude. Meanwhile, rain frequency peak (Fig. 6f) and total precipitation (Fig. 6g) go through a substantial latitudinal migration over the course of the year, and their annual cycles are as large as their annual mean values (with magnitudes similar to those over ocean). In the subtropics, the annual cycle of rain

amount peak is similar over land and ocean: present but weak compared to annual mean values. Rain frequency peak and total precipitation show large seasonal variations in magnitude in the subtropics of both hemispheres.

Maps of annual-mean rain amount peak and rain frequency peak are shown in Fig. 7, with total rainfall

superimposed for context. The geographical pattern of the rain amount peak differs considerably from that of total precipitation (Fig. 7a), while the rain frequency peak follows the total precipitation very closely (Fig. 7b). The highest values of rain amount peak exceed 50 mm day^{-1} ; regions of the highest rain amount peak values are found on the edges of regions with the highest total precipitation, outlined by the 4 mm day^{-1} contour (e.g., over India, Southeast Asia, and the Pacific coast of Mexico in the NH and northern Australia, southeastern South America, and the east coast of southern Africa in the SH). Regions with the highest total precipitation have only moderate rain amount peak values; for example, no region with greater than 7 mm day^{-1} of total precipitation has a rain amount peak of greater than 35 mm day^{-1} . Some regions of low total precipitation also have low rain amount peak values ($<5 \text{ mm day}^{-1}$), such as the tropical and subtropical southeastern Pacific, the subtropical South Atlantic, and the Himalayas. However, other regions of low total precipitation have high rain amount peak values ($10\text{--}50 \text{ mm day}^{-1}$), such as western Australia and the adjacent subtropical southeastern Indian Ocean, as well as the subtropical northeastern Atlantic. Some of the driest regions ($<1 \text{ mm day}^{-1}$ total rainfall) contain adjacent grid cells of high and low rain amount peak values; this noisiness is due to the fact that just a few rainfall events dominate the record and is thus attributable to sampling. In contrast to rain amount peak, the highest rain frequency peak values ($20\text{--}30 \text{ mm day}^{-1}$) occur within the tropics, particularly the Pacific ITCZ and the Indian Ocean. Most of these occur within the 4 mm day^{-1} contour of total precipitation.

In summary, Fig. 7 shows contrasting geographical patterns of rain amount peak and rain frequency peak. In regions of high rain amount peak, rain is heavy when it falls, but it falls infrequently enough that total precipitation is not particularly high. The regions of highest total precipitation are characterized by more frequent but moderate rainfall rates. This is consistent with Venugopal and Wallace (2016), who examined similar metrics for 3-hourly TRMM 3B42, and Dai et al. (2007), who analyzed total frequency and total intensity of rain as opposed to the metrics of the peaks of the distributions introduced here.

Another way to look at the relationships among rain amount peak, rain frequency peak, and total precipitation is to form scatterplots among these quantities (Fig. 8); we use annual-mean data for each grid box equatorward of 40° latitude. There is little correlation between rain frequency peak and rain amount peak, although the rain amount peak is always at least as large as rain frequency peak (Fig. 8a). The relationship

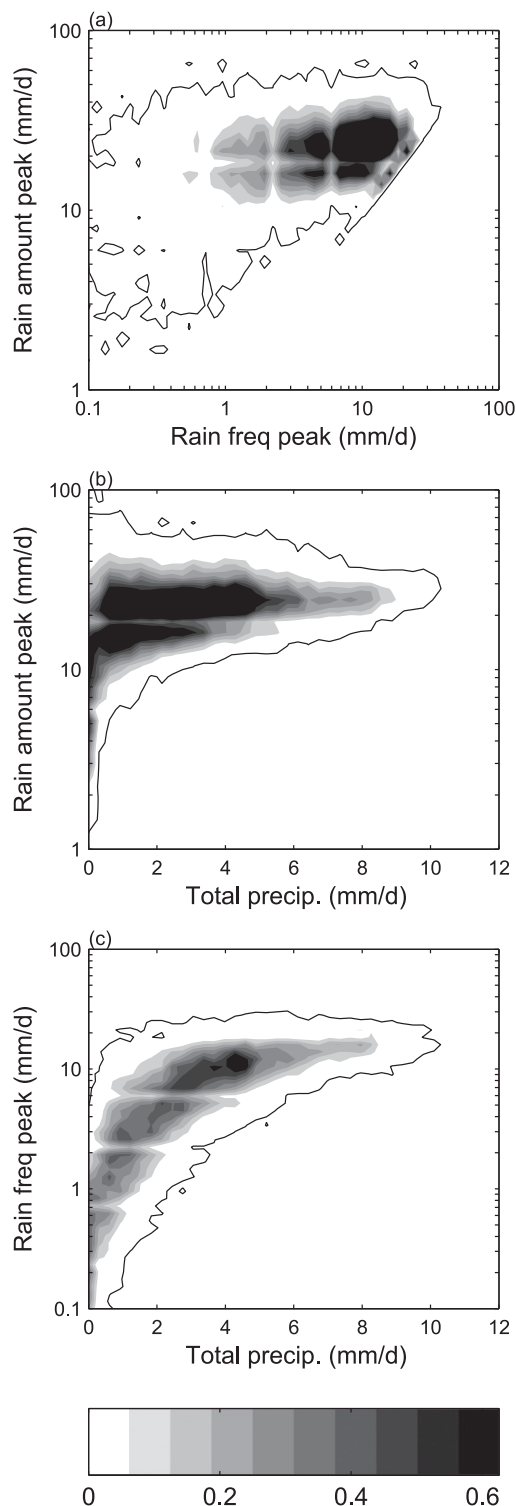


FIG. 8. Scatterplot density (%) of annual mean (a) rain amount peak vs rain frequency peak, (b) rain amount peak vs total precipitation, and (c) rain frequency peak vs total precipitation, based on GPCP 1DD data equatorward of 40° latitude. A contour line at 0.0125% is included.

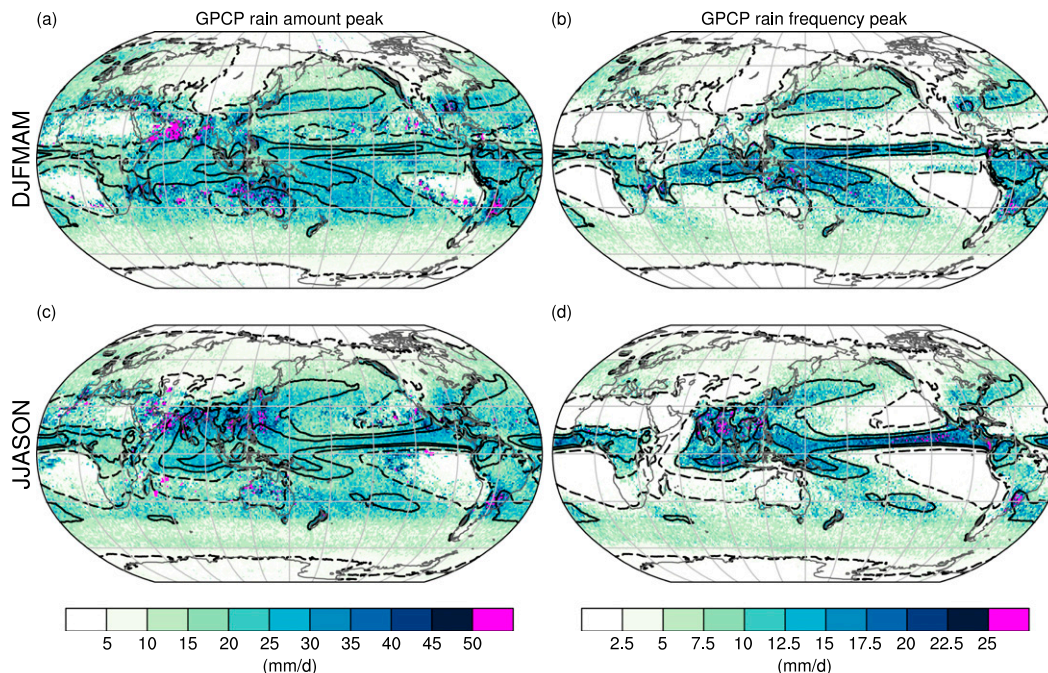


FIG. 9. As in Fig. 7, but for two half-year seasons (a),(b) December–May and (c),(d) June–November.

between rain amount peak and total precipitation is nonlinear: for small values of total precipitation, rain amount peak can be either high or low (ranging from 1 to 70 mm day^{-1} for total precipitation of $<1 \text{ mm day}^{-1}$), while for the highest values of total precipitation, the rain amount peak is moderate (rain amount peak of 20 mm day^{-1} for total precipitation of 10 mm day^{-1} ; Fig. 8b). The relationship between rain frequency peak and total precipitation is also nonlinear: rain frequency peak increases rapidly with total precipitation for values of total precipitation below 3 mm day^{-1} and then saturates at $10\text{--}20 \text{ mm day}^{-1}$ for total precipitation of $>3 \text{ mm day}^{-1}$ (Fig. 8c).

To examine the seasonal cycle of the spatial patterns of rain amount peak and rain frequency peak, we subdivide the year into two halves (December–May and June–November; Fig. 9). These extended seasons emphasize the times of year when the total tropical rainfall is greatest: December–May in the SH and June–November in the NH. In austral summer and fall, the highest values of rain amount peak are found in the latitude band between 10° and 30° in both hemispheres, particularly over Australia extending westward over the Indian Ocean to the southern tip of South Africa and near Uruguay in South America; these locations are situated south of the regions with the greatest total precipitation (Fig. 9a). In addition, high rain amount peak values occur over the northern Indian Ocean, well north of the region of high total rainfall. In contrast, the

largest values of rain frequency peak are contained within the band of greatest total precipitation (Fig. 9b). In boreal summer and fall, the highest values of rain amount peak are found in the NH between 10° and 30°N , primarily over India and Southeast Asia (Fig. 9c). While these areas occur within the region of high total precipitation, they are located north of the maximum total precipitation, unlike the high values of rain frequency peak, which are contained entirely within the contours of maximum total precipitation (Fig. 9d).

In summary, the rain frequency peak varies in a similar way to total precipitation both spatially and over the seasonal cycle. The rain amount peak shows less correspondence with total precipitation and exhibits maximum values in regions of infrequent precipitation.

c. Rain amount width

Figures 6d,h show the seasonal cycle of zonal-mean rain amount width over ocean and land. The rain amount width varies inversely with total precipitation (cf. Figs. 6c,d, and Figs. 6g,h). It has a minimum in the tropics and a maximum that varies with season in the subtropics over both land and ocean. Over ocean, the seasonal cycle is relatively muted. Maximum rain amount width values ($2.3\text{--}2.7$) occur in the latitude band $10^\circ\text{--}30^\circ\text{N}$ and in the Arctic. Over land, rain amount width varies between 2 and 3 and shows a pronounced latitudinal migration with the seasonal cycle, reaching the largest values in the subtropics.

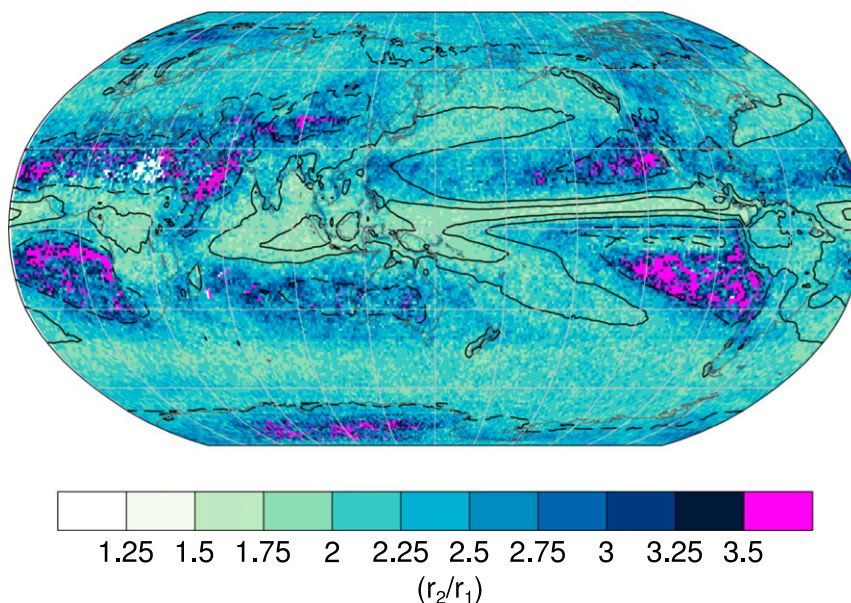


FIG. 10. As in Fig. 7, but for rain amount width (unitless). See text for definition.

The map of annual-mean rain amount width is shown in Fig. 10, along with the same contours of total precipitation as Figs. 7 and 9. The geographical pattern of annual-mean rain amount width varies inversely with total precipitation, consistent with the behavior of zonal-mean rain amount width. That is, regions with low total precipitation have wide rain amount distributions, and vice versa. In regions of low total precipitation including the subtropical dry zones, the Himalayas, and Antarctica, rain amount width reaches maxima of over 3.5 (regions shown in white over the eastern Sahara are grid points where there were too few days with rain to reliably calculate the width). In tropical regions of high total precipitation, the rain amount width reaches its minimum values of 1.5–2.

The inverse relationship between total precipitation and rain amount width is also evident in each half-year

season (Fig. 11). In the southeastern Pacific and Atlantic, the region of high rain amount width is more concentrated in austral summer–fall (Fig. 11a) when the dry zone is more contracted compared to austral winter–spring (Fig. 11b). High rain amount width persists through both seasons in the south Indian Ocean. Over the NH midlatitude continents (e.g., Siberia and western North America), higher values of rain amount width are found over the continental interiors in winter and spring (up to 3.5) than in summer and fall (around 2).

5. Comparison with TRMM

To account for differences between observational products, we examine data from TRMM 3B42 to compare against our analysis of GPCP. The two precipitation datasets (GPCP 1DD and TRMM 3B42) are

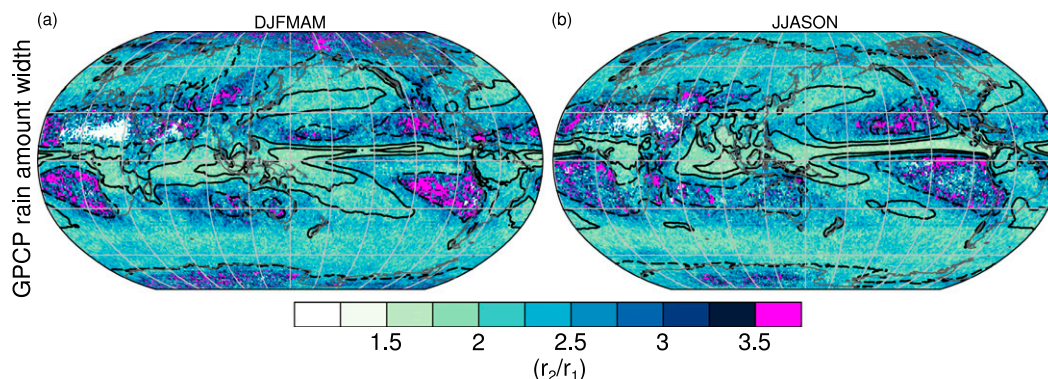


FIG. 11. As in Fig. 10, but for two half-year seasons (a) December–May and (b) June–November.

both merged satellite-gauge gridded products, so their comparison likely provides only a lower bound on observational uncertainty rather than a full accounting of it. A more thorough assessment of observational uncertainty associated with a wide range of precipitation datasets can be found in [Gehne et al. \(2016\)](#) and [Herold et al. \(2016\)](#). However, neither study examined the metrics shown here: [Gehne et al. \(2016\)](#) focused primarily on monthly mean precipitation over North America, with a brief examination of the distribution of rain in that region, while [Herold et al. \(2016\)](#) assessed aggregated (total) intensity of precipitation over land.

[Figure 12](#) shows the spatially averaged distributions of annual-mean rain amount and rain frequency over TRMM's coverage area 50°N–50°S for both TRMM and GPCP. TRMM's rain amount distribution is centered at heavier rain rates than GPCP's ([Fig. 12a](#)), and it is wider. Our metrics quantify this: the rain amount peak is 28 mm day⁻¹ for TRMM and only 21 mm day⁻¹ for GPCP, and the width of the rain amount distribution in TRMM is 2.5 compared to 2.1 in GPCP. In addition, the shape of the rain frequency distribution differs between the two datasets. TRMM has more light rain days than GPCP and accordingly has fewer dry days (47% compared to 56%). TRMM also exhibits slightly larger rain frequencies at the highest rain rates (>30 mm day⁻¹) than GPCP.

[Figure 13](#) shows maps of annual-mean rain amount peak, rain frequency peak, and rain amount width from TRMM. Note that the color bar span is doubled for the TRMM's rain amount peak compared to GPCP's (reaching 100 rather than 50 mm day⁻¹), to accommodate its larger values while preserving the spatial pattern. While the magnitude of the rain amount peak differs between the two datasets, the spatial patterns are consistent in showing maximum values of the rain amount peak at the margins of the regions of greatest total precipitation ([Fig. 13a](#)). One important difference between the two datasets is that in TRMM the highest rain amount peak values occur over ocean, while in GPCP they occur over both ocean and land. The rain frequency peak has generally similar magnitudes in TRMM and GPCP, and the geographical correspondence with total precipitation remains ([Fig. 13b](#)). However, in regions of moderate total precipitation in the subtropics, rain frequency peak is generally <2.5 mm day⁻¹ in TRMM compared to 2.5–15 mm day⁻¹ in GPCP. As in GPCP, the rain amount width in TRMM varies inversely with total precipitation ([Fig. 13c](#)). Values of rain amount width are larger for TRMM than for GPCP, consistent with spatial annual-mean distribution ([Fig. 12](#)).

In summary, GPCP and TRMM datasets agree on the general spatial pattern of the rain amount peak, many

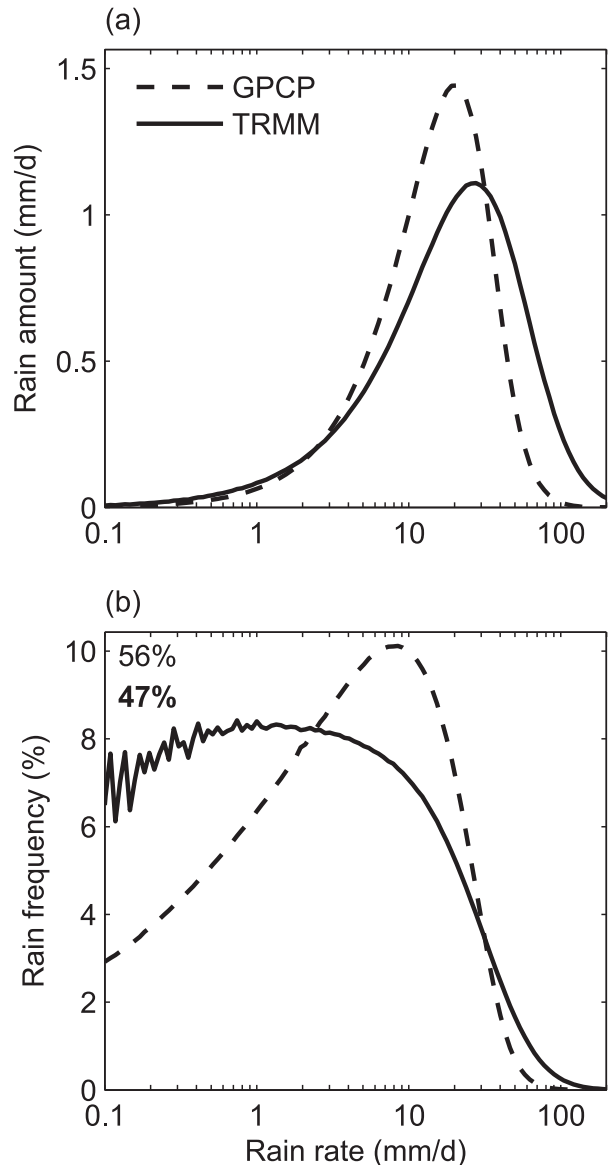


FIG. 12. As in [Fig. 2](#), but for data from TRMM 3B42 (solid curves) and GPCP 1DD (dashed curves), averaged between 50°N and 50°S.

aspects of the spatial pattern of rain frequency peak, and the inverse relationship between rain amount and total precipitation. On the other hand, the magnitude of rain amount peak and rain amount width is much larger in TRMM than in GPCP.

6. Rain frequency: Some concerns and comparison with CESM1

In the previous section, we saw that GPCP and TRMM agree more closely on the spatial annual-mean rain amount distribution than on the rain frequency

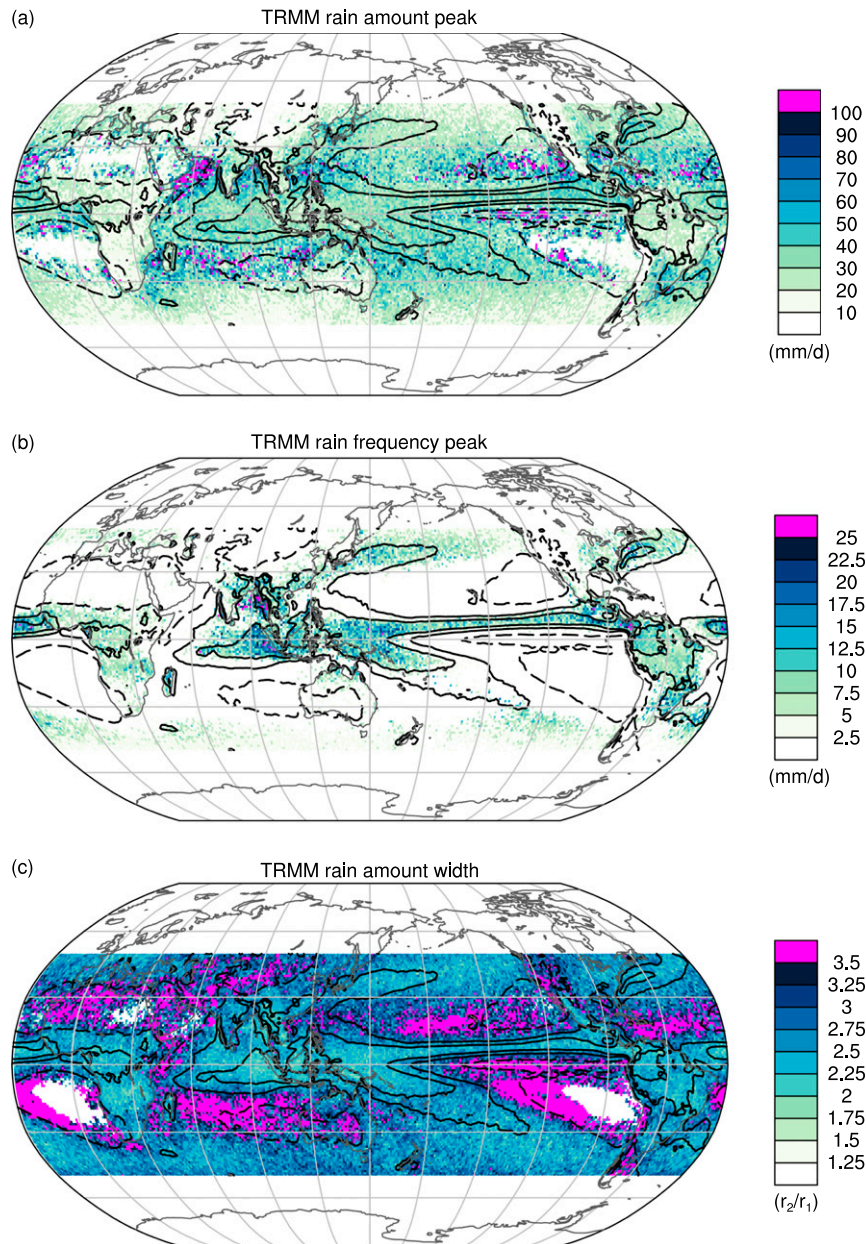


FIG. 13. Maps of climatological annual mean (a) rain amount peak (mm day^{-1}), (b) rain frequency peak (mm day^{-1}), and (c) rain amount width (unitless) from TRMM 3B42 data during January 1998–October 2015. Contours of total precipitation follow Fig. 7.

distribution. In this section we explore the rain frequency width for GPCP and TRMM. In addition, we analyze the CESM1 simulation introduced in section 2, which indicates that the characteristics of the observational uncertainty of the GPCP and TRMM datasets at light rain rates could lead to qualitative deficiencies in the observed rain frequency distribution.

Maps of annual mean rain frequency width for GPCP and TRMM are compared in Fig. 14. For GPCP

(Fig. 14a), the rain frequency width varies inversely with total precipitation, similar to rain amount width (Fig. 10), although with generally larger values. In contrast, TRMM's rain frequency width (Fig. 14b) behaves quite differently from its rain amount width (cf. Fig. 13c). It reaches local minima in regions of high total precipitation, just as its rain amount width does, but other large regions do not display the inverse relationship with total precipitation. For example, the subtropical dry zones have

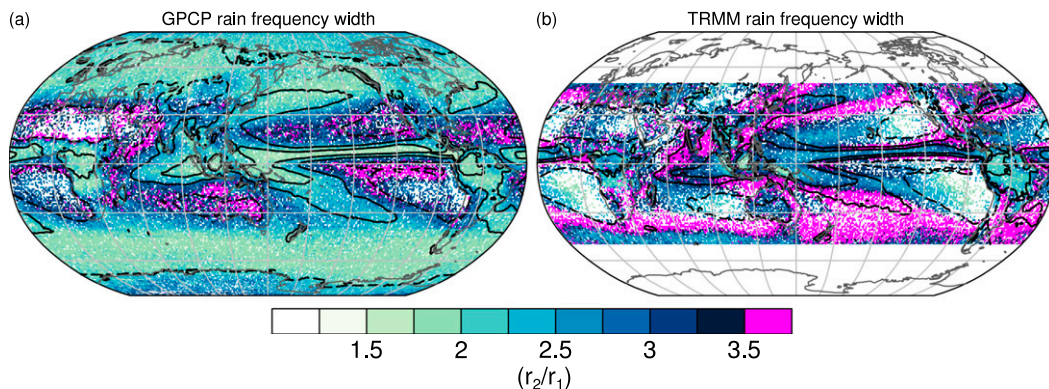


FIG. 14. Maps of climatological annual mean rain frequency width (unitless) from (a) GPCP 1DD and (b) TRMM 3B42. Contours of total precipitation follow Fig. 7.

minima in rain frequency width. We speculate that these differences arise from assumptions in the way the datasets are constructed; as far as we are aware, it is not clear if one is more correct than the other.

The fundamental differences in the spatial pattern of rain frequency width between the two datasets decrease our confidence in other aspects of the observed rain frequency distribution. To adjudicate this discrepancy, we consult the distribution of rain from CESM1. While climate models are not reality, they have the advantage over observations of perfect reporting in space and time.

Figures 15a,b shows the annual, zonal-mean rain amount distributions for GPCP with TRMM. Compared to GPCP, TRMM's rain amount distribution is wider, shows a stronger latitudinal variation, and reaches its maximum at a higher rain rate. However, their qualitative features are similar. In contrast, the rain frequency distribution differs more between the two datasets (Figs. 15d,e). While GPCP's rain frequency distribution could be largely anticipated from its rain amount distribution, TRMM's rain frequency distribution has higher values at light rain rates ($<1 \text{ mm day}^{-1}$) in the tropics and subtropics compared to GPCP than would be anticipated from its rain amount distribution.

The annual, zonal-mean rain amount distribution for CESM1 (Fig. 15c) has many characteristics in common with GPCP and TRMM: a maximum in the tropics, minima in the subtropics, local maxima in the mid-latitudes, and a rain amount peak that is nearly invariant with latitude. Its rain amount distribution maxima are closer to GPCP than TRMM. However, the negative skewness of the distribution is weaker in CESM1 compared to either observational dataset. On the other hand, the rain frequency distribution exhibits notable differences from the observations (Fig. 15f). The most striking discrepancy is frequency maxima at light rain rates in the subtropics of both hemispheres in the model,

which are absent in GPCP and muted in TRMM. These local maxima at light rain rates correspond to stratocumulus regions of the subtropical dry zones and are also present in other climate models (not shown).

Figure 16 shows maps of annual-mean rain amount peak, rain frequency peak, rain amount width, and rain frequency width for CESM1. The rain amount peak (Fig. 16a) is smaller in magnitude than either GPCP or TRMM (recall Figs. 7a and 13a, respectively; note that the color bar for CESM1 covers half of GPCP's range and a quarter of TRMM's). Its highest values occur just outside the 4 mm day^{-1} contour of the total precipitation, as in observations, but the geographical location of these values differs. Specifically, the rain amount peak reaches maxima poleward of the mid-latitude storm tracks and south of the SPCZ and lacks the local maxima over the tropical continents (including India, Southeast Asia, and Australia). The rain frequency peak (Fig. 16b; cf. Figs. 7b and 13b) also has a smaller magnitude than observations (note that the color bar covers half the range of that used for GPCP and TRMM). Its spatial pattern has both similarities and differences between the model and observations. As in observations, the highest values of rain frequency peak occur in the regions of high total precipitation. Unlike observations (especially GPCP), the rain frequency peak rapidly drops to very light values outside of the regions of heavy total precipitation since the model has many more light rain days than the observational datasets (as we saw in Fig. 15). The rain amount width (Fig. 16c; cf. Figs. 10 and 13a) reaches its highest values in the subtropical oceans, the North Pacific and south Indian Oceans, and has minima both in regions of high total precipitation and in regions of low total precipitation; in this sense it is more similar to TRMM than GPCP. The rain frequency width (Fig. 16d; cf. Fig. 14) reaches higher values than either TRMM or GPCP,

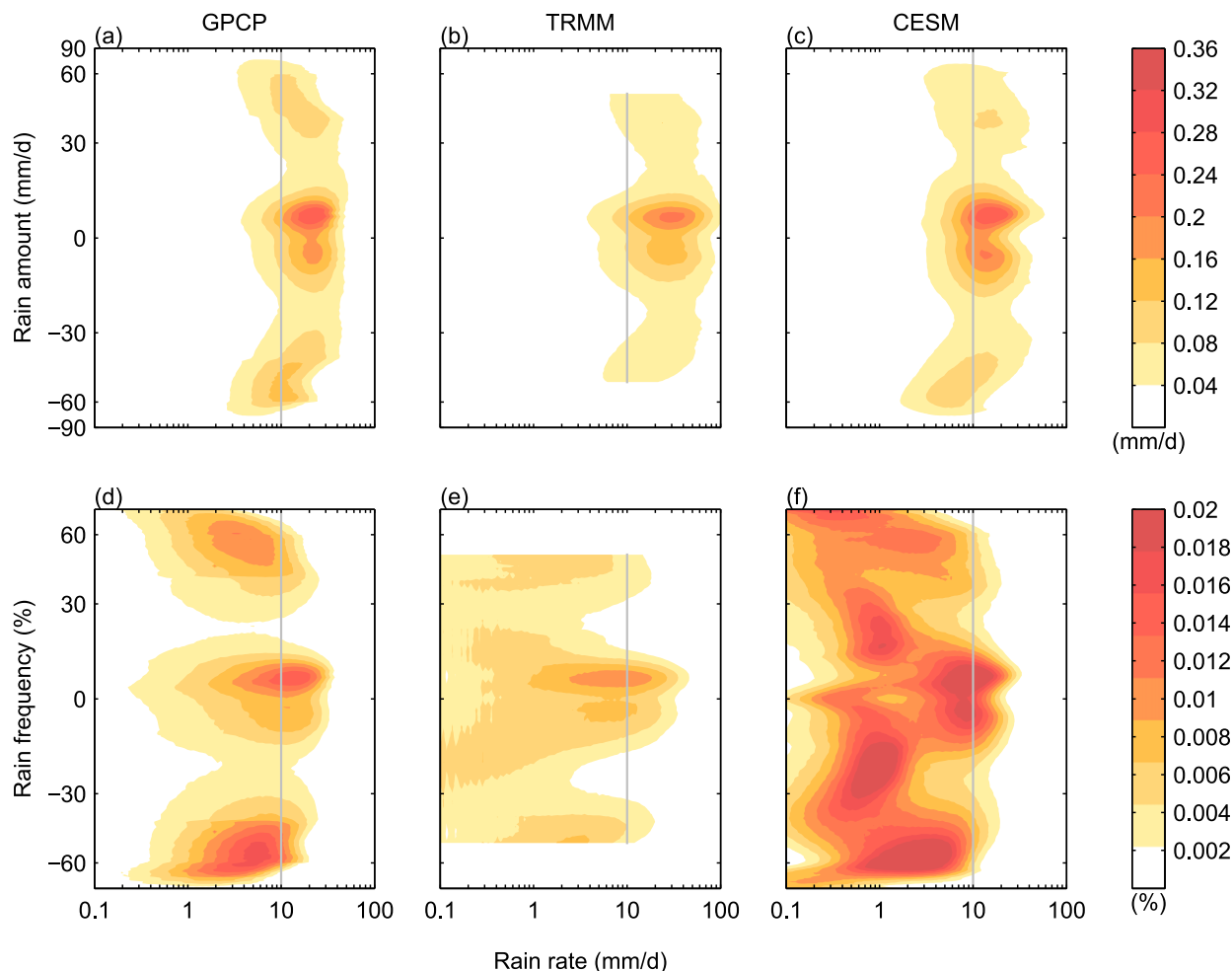


FIG. 15. Comparison between climatological zonal annual-mean distributions of (top) rain amount (mm day^{-1}) and (bottom) rain frequency (%) for (a),(d) GPCP 1DD, (b),(e) TRMM 3B42 (coarsened to 1° resolution), and (c),(f) CESM1.

consistent with its higher frequency of light rain days, which play little role in the rain amount distribution width. It also shares more characteristics with TRMM than GPCP, including reaching minima rather than maxima in dry zones and reaching maxima rather than minima near the midlatitude storm tracks.

7. Discussion

As we have just shown, CESM1 has a much higher frequency of light rain than either GPCP or TRMM and correspondingly lower values of rain frequency peak, especially over the subtropical oceans. While we know that climate models disagree about some of the physical processes controlling stratocumulus clouds in the eastern side of the subtropical ocean basins (e.g., Fasullo and Trenberth 2012; Medeiros et al. 2012; Sherwood et al. 2014), we also know that the satellite measurements

incorporated into GPCP and TRMM are not sensitive enough to light precipitation below about 1 mm day^{-1} (Behrangi et al. 2012, 2014), which are especially important for obtaining the correct rain frequency distribution (Huffman et al. 2001, 2007). Other datasets such as *CloudSat* radar and *CALIPSO* lidar measurements accurately represent the frequency of occurrence of rain, including very light rain (e.g., Lebsock and L'Ecuyer 2011), but cannot accurately estimate the rain rate for moderate to heavy precipitation. They also have insufficient sampling to form the basis for high spatial and temporal resolution gridded datasets like GPCP and TRMM. Even considering the frequency of light precipitation observed by *CloudSat*, it is still likely that climate models overestimate the frequency of light rainfall (Stephens et al. 2010). However, more and improved observations of light precipitation are needed to better understand this discrepancy. The new Global

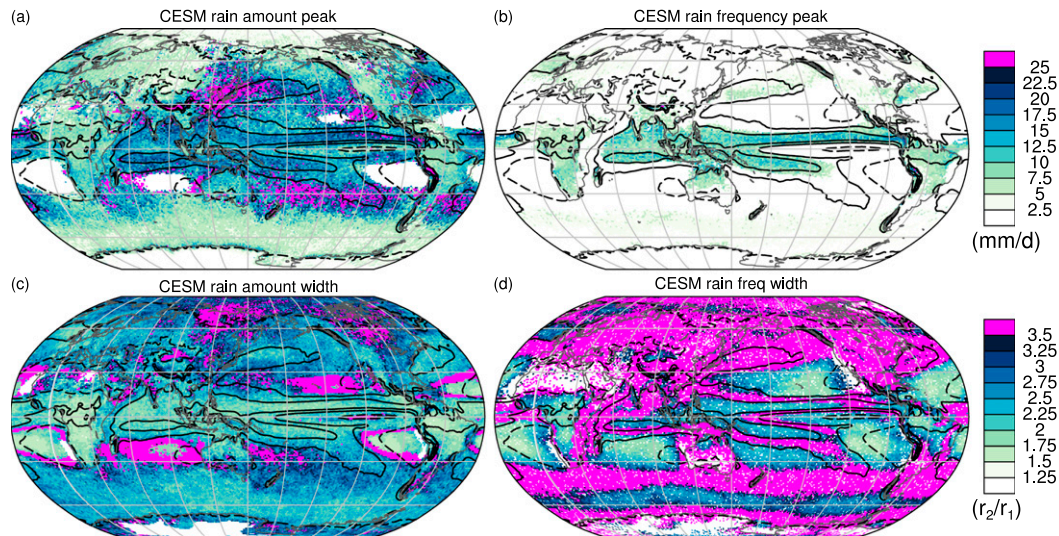


FIG. 16. Maps of climatological annual mean (a) rain amount peak, (b) rain frequency peak, (c) rain amount width, and (d) rain frequency width from CESM1. Contours of total precipitation follow Fig. 7.

Precipitation Measurement (GPM; Hou et al. 2014) mission makes some optimistic claims about observing light precipitation, but our brief comparison between IMERG and TRMM over their common period of record (not shown) indicates little difference between them.

The comparison between the precipitation distributions from GPCP and TRMM and the CESM1 model simulation (which is representative of other comprehensive climate model simulations in the aspects we have examined; not shown) indicates that there are important gaps in our knowledge of the distribution of rain frequency, including the extent to which precipitation is accurately represented in observational datasets. It also shows that there is better agreement on the rain amount distribution than on the rain frequency distribution. The rain amount distribution focuses on the bulk of total precipitation, which makes it an easy and thus conservative target. That is, it is relatively easy to constrain energetically in models and relatively hard to miss with an observing system. For this reason, we have emphasized analysis of the rain amount distribution over the rain frequency distribution. Our analysis shows that agreement between the observational datasets is particularly high for spatial and seasonal variations in the rain amount distribution, rather than for absolute magnitudes of the various metrics. That said, improving the state of our knowledge of the absolute magnitude of rain amount and also the rain frequency distribution in general would be a worthy endeavor. For example, rain frequency can play a more important role than total precipitation for plants in the Amazon (Cook et al. 2012) and for soil crusts in desert regions (Belnap et al. 2004).

8. Concluding remarks

We have introduced metrics to quantify typical daily precipitation accumulation from the distribution of rain. The metrics include the rain amount peak, which is the rate where the most rain falls; the rain frequency peak, which is the most frequent nonzero rain rate; and the rain amount width, which is a measure of the variability of typical precipitation accumulation. These metrics portray characteristics associated with typical daily precipitation. In this way, our study differs from previous investigations, which tend to emphasize characteristics of extreme precipitation or aggregations over the entire distribution of rainfall. We applied these three metrics to the GPCP 1° daily dataset, which has global coverage from October 1996 to October 2015. In addition to examining the zonal-mean distribution of rain amount and rain frequency over land and ocean, we showed the geographical patterns and seasonal variations of our three “typical” precipitation metrics and compared them against total precipitation. We repeated the analysis using TRMM 3B42, another merged satellite-gauge product coarsened to a 1° resolution for comparison, to provide a lower bound on the uncertainty between datasets. Finally, we compared the typical precipitation metrics from observational datasets with those from a climate model simulation (CESM1). To the best of our knowledge, this is the first study that provides a comprehensive description of the global spatial pattern and seasonal cycle of typical precipitation accumulation at daily or subdaily time scales from more than one observational dataset.

In general, there is little variation in the rate at which rain falls across latitudes, surface type and season. However, this zonal-mean picture belies a rich longitudinal structure. The geographical pattern and seasonal variation of rain frequency peak largely follow those of total precipitation, while rain amount peak reaches its highest values on the poleward margins of the total precipitation maxima in the tropics. The highest values of rain amount peak are found over southern Asia, the southeastern United States, the southwestern Indian Ocean, northern Australia, and eastern-central South America. Rain amount width exhibits an inverse relationship to total precipitation in both its spatial pattern and seasonal variation. Comparison with TRMM shows that differences between precipitation datasets can be large, even when they incorporate similar raw measurements. While GPCP and TRMM show broadly similar spatial patterns of rain amount peak, they have large quantitative differences. Both datasets show an inverse relationship between total precipitation and rain amount width, but they show the inconsistent behavior for rain frequency width. Comparison with the CESM1 simulation indicates that in order to validate models, observational datasets incorporating measurements of light rain are needed.

There remains much to learn from examining the characteristics of typical daily rainfall. Beyond our focus on characterizing their climatology in observations, these metrics will also be useful for evaluating models [see related work by [Kooperman et al. \(2016\)](#)]. They could also be used to assess changes in the distribution of precipitation with global warming in models and eventually in observational datasets, although we hesitate to undertake this with the short records considered here. Finally, while we have focused on distributions of daily precipitation, these metrics can also be applied to datasets with higher temporal frequency (e.g., [Venugopal and Wallace 2016](#)).

Acknowledgments. We thank Drs. Dennis Hartmann and Mike Wallace for useful discussions during the course of this work and the anonymous reviewers for their constructive comments and suggestions. AGP was funded by NCAR's Advanced Studies Program and the University of Colorado CIRES Visiting Fellow postdoctoral research fellowships and the Regional and Global Climate Modeling Program of the U.S. Department of Energy's Office of Science, Cooperative Agreement DE-FC0297ER62402. Software to calculate the metrics is available at <http://github.com/apendergrass/rain-metrics-python>. NASA generously provides GPCP 1DD data at <ftp://meso.gsfc.nasa.gov/pub/1dd-v1.2> and TRMM 3B42 data at <https://pmm.nasa.gov/data-access/downloads/trmm>.

REFERENCES

- Allen, M. R., and W. J. Ingram, 2002: Constraints on future changes in climate and the hydrologic cycle. *Nature*, **419**, 224–232, doi:[10.1038/nature01092](https://doi.org/10.1038/nature01092); Corrigendum, **489**, 590, doi:[10.1038/nature11456](https://doi.org/10.1038/nature11456).
- Amante, C., and B. W. Eakins, 2009: ETOPO1 1 arc-minute global relief model: Procedures, data sources and analysis. NOAA Tech. Memo. NESDIS NGDC-24, 25 pp. [Available online at <https://www.ngdc.noaa.gov/mgg/global/relief/ETOPO1/docs/ETOPO1.pdf>.]
- Behrangi, A., M. Lebsock, S. Wong, and B. Lambrigtsen, 2012: On the quantification of oceanic rainfall using spaceborne sensors. *J. Geophys. Res.*, **117**, D20105, doi:[10.1029/2012JD017979](https://doi.org/10.1029/2012JD017979).
- , G. Stephens, R. F. Adler, G. J. Huffman, B. Lambrigtsen, and M. Lebsock, 2014: An update on the oceanic precipitation rate and its zonal distribution in light of advanced observations from space. *J. Climate*, **27**, 3957–3965, doi:[10.1175/JCLI-D-13-00679.1](https://doi.org/10.1175/JCLI-D-13-00679.1).
- Belnap, J., S. L. Phillips, and M. E. Miller, 2004: Response of desert biological soil crusts to alterations in precipitation frequency. *Oecologia*, **141**, 306–316, doi:[10.1007/s00442-003-1438-6](https://doi.org/10.1007/s00442-003-1438-6).
- Biasutti, M., and S. E. Yuter, 2013: Observed frequency and intensity of tropical precipitation from instantaneous estimates. *J. Geophys. Res. Atmos.*, **118**, 9534–9551, doi:[10.1002/jgrd.50694](https://doi.org/10.1002/jgrd.50694).
- Chen, M., R. E. Dickinson, X. Zeng, and A. N. Hahmann, 1996: Comparison of precipitation observed over the continental United States to that simulated by a climate model. *J. Climate*, **9**, 2233–2249, doi:[10.1175/1520-0442\(1996\)009<2233:COPOOT>2.0.CO;2](https://doi.org/10.1175/1520-0442(1996)009<2233:COPOOT>2.0.CO;2).
- Cook, B., N. Zeng, and J. H. Yoon, 2012: Will Amazonia dry out? Magnitude and causes of change from IPCC climate model projections. *Earth Interact.*, **16**, doi:[10.1175/2011EI398.1](https://doi.org/10.1175/2011EI398.1).
- Dai, A., 2001: Global precipitation and thunderstorm frequencies. Part I: Seasonal and interannual variations. *J. Climate*, **14**, 1092–1111, doi:[10.1175/1520-0442\(2001\)014<1092:GPATFP>2.0.CO;2](https://doi.org/10.1175/1520-0442(2001)014<1092:GPATFP>2.0.CO;2).
- , 2006: Precipitation characteristics in eighteen coupled climate models. *J. Climate*, **19**, 4605–4630, doi:[10.1175/JCLI3884.1](https://doi.org/10.1175/JCLI3884.1).
- , X. Lin, and K.-L. Hsu, 2007: The frequency, intensity, and diurnal cycle of precipitation in surface and satellite observations over low- and mid-latitudes. *Climate Dyn.*, **29**, 727–744, doi:[10.1007/s00382-007-0260-y](https://doi.org/10.1007/s00382-007-0260-y).
- Englehart, P. J., and A. V. Douglas, 1985: A statistical analysis of precipitation frequency in the conterminous United States, including comparisons with precipitation totals. *J. Climate Appl. Meteor.*, **24**, 350–362, doi:[10.1175/1520-0450\(1985\)024<0350:ASAOPF>2.0.CO;2](https://doi.org/10.1175/1520-0450(1985)024<0350:ASAOPF>2.0.CO;2).
- Fasullo, J. T., and K. E. Trenberth, 2012: A less cloudy future: The role of subtropical subsidence in climate sensitivity. *Science*, **338**, 792–794, doi:[10.1126/science.1227465](https://doi.org/10.1126/science.1227465).
- Gehne, M., T. M. Hamill, G. N. Kiladis, and K. E. Trenberth, 2016: Comparison of global precipitation estimates across a range of temporal and spatial scales. *J. Climate*, **29**, 7773–7795, doi:[10.1175/JCLI-D-15-0618.1](https://doi.org/10.1175/JCLI-D-15-0618.1).
- Held, I. M., and B. J. Soden, 2006: Robust responses of the hydrologic cycle to global warming. *J. Climate*, **19**, 5686–5699, doi:[10.1175/JCLI3990.1](https://doi.org/10.1175/JCLI3990.1).
- Herold, N., L. V. Alexander, M. G. Donat, S. Contractor, and A. Becker, 2016: How much does it rain over land? *Geophys. Res. Lett.*, **43**, 341–348, doi:[10.1002/2015GL066615](https://doi.org/10.1002/2015GL066615).
- Hou, A. Y., and Coauthors, 2014: The Global Precipitation Measurement mission. *Bull. Amer. Meteor. Soc.*, **95**, 701–722, doi:[10.1175/BAMS-D-13-00164.1](https://doi.org/10.1175/BAMS-D-13-00164.1).

- Huffman, G. J., and D. T. Bolvin, 2013: Version 1.2 GPCP one-degree daily precipitation data set documentation. NASA Goddard Space Flight Center Rep., 27 pp. [Available online at ftp://meso.gsfc.nasa.gov/pub/1dd-v1.2/1DD_v1.2_doc.pdf.]
- , R. F. Adler, M. M. Morrissey, D. T. Bolvin, S. Curtis, R. Joyce, B. McGavock, and J. Susskind, 2001: Global precipitation at one-degree daily resolution from multisatellite observations. *J. Hydrometeor.*, **2**, 36–50, doi:10.1175/1525-7541(2001)002<0036:GPAODD>2.0.CO;2.
- , and Coauthors, 2007: The TRMM Multisatellite Precipitation Analysis (TMPA): Quasi-global, multiyear, combined-sensor precipitation estimates at fine scales. *J. Hydrometeor.*, **8**, 38–55, doi:10.1175/JHM560.1.
- Hurrell, J. W., and Coauthors, 2013: The Community Earth System Model: A framework for collaborative research. *Bull. Amer. Meteor. Soc.*, **94**, 1339–1360, doi:10.1175/BAMS-D-12-00121.1.
- Kay, J. E., and Coauthors, 2015: The Community Earth System Model (CESM) large ensemble project: A community resource for studying climate change in the presence of internal climate variability. *Bull. Amer. Meteor. Soc.*, **96**, 1333–1349, doi:10.1175/BAMS-D-13-00255.1.
- Kooperman, G. J., M. S. Pritchard, M. A. Burt, M. D. Branson, and D. A. Randall, 2016: Robust effects of cloud superparameterization on simulated daily rainfall intensity statistics across multiple versions of the Community Earth System Model. *J. Adv. Model. Earth Syst.*, **8**, 140–165, doi:10.1002/2015MS000574.
- Kummerow, C., and L. Giglio, 1995: A method for combining passive microwave and infrared rainfall observations. *J. Atmos. Oceanic Technol.*, **12**, 33–45, doi:10.1175/1520-0426(1995)012<0033:AMFCPM>2.0.CO;2.
- Lebsock, M. D., and T. S. L'Ecuyer, 2011: The retrieval of warm rain from *CloudSat*. *J. Geophys. Res.*, **116**, D20209, doi:10.1029/2011JD016076.
- Medeiros, B., D. L. Williamson, C. Hannay, and J. G. Olson, 2012: Southeast Pacific stratocumulus in the Community Atmosphere Model. *J. Climate*, **25**, 6175–6192, doi:10.1175/JCLI-D-11-00503.1.
- Menne, M. J., I. Durre, R. S. Vose, B. E. Gleason, and T. G. Houston, 2012a: An overview of the Global Historical Climatology Network-Daily Database. *J. Atmos. Oceanic Technol.*, **29**, 897–910, doi:10.1175/JTECH-D-11-00103.1.
- , and Coauthors, 2012b: Global Historical Climatology Network - daily (GHCN-Daily), version 3.21. NOAA National Climatic Data Center, accessed 9 July 2015, doi:10.7289/V5D21VHZ.
- Min, S. K., X. Zhang, F. W. Zwiers, and G. C. Hegerl, 2011: Human contribution to more-intense precipitation extremes. *Nature*, **470**, 378–381, doi:10.1038/nature09763.
- Pall, P., M. R. Allen, and D. A. Stone, 2007: Testing the Clausius–Clapeyron constraint on changes in extreme precipitation under CO₂ warming. *Climate Dyn.*, **28**, 351–363, doi:10.1007/s00382-006-0180-2.
- Pendergrass, A. G., and D. L. Hartmann, 2014a: Two modes of change of the distribution of rain. *J. Climate*, **27**, 8357–8371, doi:10.1175/JCLI-D-14-00182.1.
- , and —, 2014b: Changes in the distribution of rain frequency and intensity in response to global warming. *J. Climate*, **27**, 8372–8383, doi:10.1175/JCLI-D-14-00183.1.
- Petty, G. W., 1995: Frequencies and characteristics of global oceanic precipitation from shipboard present-weather reports. *Bull. Amer. Meteor. Soc.*, **76**, 1593–1616, doi:10.1175/1520-0477(1995)076<1593:FACOGO>2.0.CO;2.
- Ricko, M., R. F. Adler, and G. J. Huffman, 2016: Climatology and interannual variability of quasi-global intense precipitation using satellite observations. *J. Climate*, **29**, 5447–5468, doi:10.1175/JCLI-D-15-0662.1.
- Sherwood, S. C., S. Bony, and J. L. Dufresne, 2014: Spread in model climate sensitivity traced to atmospheric convective mixing. *Nature*, **505**, 37–42, doi:10.1038/nature12829.
- Stephens, G. L., and Coauthors, 2010: Dreary state of precipitation in global models. *J. Geophys. Res.*, **115**, D24211, doi:10.1029/2010JD014532.
- Stone, D. A., A. J. Weaver, and F. W. Zwiers, 2000: Trends in Canadian precipitation intensity. *Atmos.–Ocean*, **38**, 321–347, doi:10.1080/07055900.2000.9649651.
- Sun, Y., S. Solomon, A. Dai, and R. W. Portmann, 2006: How often does it rain? *J. Climate*, **19**, 916–934, doi:10.1175/JCLI3672.1.
- , —, —, and —, 2007: How often will it rain? *J. Climate*, **20**, 4801–4818, doi:10.1175/JCLI4263.1.
- Venugopal, V., and M. J. Wallace, 2016: Climatology of contribution-weighted tropical rain rates based on TRMM 3B42. *Geophys. Res. Lett.*, **43**, 10 439–10 447, doi:10.1002/2016GL069909.
- Watterson, I. G., and M. R. Dix, 2003: Simulated changes due to global warming in daily precipitation means and extremes and their interpretation using the gamma distribution. *J. Geophys. Res.*, **108**, 4379, doi:10.1029/2002JD002928.
- Wentz, F. J., L. Ricciardulli, K. Hilburn, and C. Mears, 2007: How much more rain will global warming bring? *Science*, **317**, 233–235, doi:10.1126/science.1140746.